Engineering and Technology Journal
Journal homepage: https://etj.uotechnology.edu.iq

A comparative study of viscoelastic characteristics in polymer composite with respect to the damping performance and structural behavior

Rafal A. Hameed

Department of Materials Science, College of Science, University of Aliraqia, Baghdad, Iraq.
*Corresponding author Email: rafal.a.hameed@aliraqia.edu.iq

HIGHLIGHTS

- The impact of different polymer types on composite damping performance was evaluated.
- Structural behavior under dynamic loading was compared for various composite configurations.
- The link between viscoelastic properties and vibration absorption efficiency was identified
- Specific formulations enhanced damping while maintaining mechanical strength.

Keywords:

Viscoelastic damping
Polymer composites
Filler morphology
Dynamic mechanical analysis
Loss modulus.

ABSTRACT

This study systematically investigates the viscoelastic characteristics and damping performance of polymer composites, examining the interplay between filler morphology, matrix-filler interactions, and structural behavior. The purpose is to understand and predict how different fillers influence key viscoelastic properties to enable tailored composite design. Methods and Key Findings: Dynamic mechanical analysis (DMA) and forced vibration tests were used to characterize temperature- and frequency-dependent viscoelastic properties, including storage modulus (E′), loss modulus (E″), and damping factor (tanδ). Key results demonstrate distinct effects: Spherical calcium carbonate increased stiffness (E′) by 45% at 15 wt% loading but restricted damping (tan δ) due to agglomeration-induced stress concentrations. In contrast, core-shell rubber particles increased tan δ by 280% through interfacial slip, achieving a damping ratio (ζ) of 0.052 (2.8 times higher than neat epoxy). Nanoclay composites exhibited frequency-dependent damping anisotropy from processing alignment. Hybrid filler systems showed synergistic damping effects within the 10–50 Hz range. Optimal performance occurred at 5 wt% Al_2O_3, balancing moderate stiffness (E′ = 1.5 GPa) with peak damping (tan δ = 0.82). Microstructural analyses (SEM/AFM) correlated maximized interfacial friction and damping with an agglomerate area fraction <10%. A validated multi-scale computational model (<7% error) successfully bridged nanoscale mechanisms to macroscale performance. Significance and Applications: This work provides a predictive framework for designing next-generation composites. It enables tailored material design—prioritizing damping for applications like automotive NVH systems or stiffness for aerospace components—advancing fundamental knowledge of composite viscoelasticity and offering practical strategies for industrial vibration mitigation.

1. Introduction

Polymer composites have become crucial in contemporary engineering due to their excellent adaptability, lightweight properties, and capacity to fulfill rigorous demands in dynamic structural applications. Central to their capability is viscoelasticity—a dual-segment behavior combining viscous electricity dissipation with elastic strength storage. This intrinsic property arises from molecular mobility inside polymer chains and their interactions with embedded fillers, allowing powerful vibration mitigation important for aerospace, automobile, and precision instrumentation [1]. The damping thing ($\tan\delta$), described as the ratio of loss modulus (E'') described because the ratio of loss modulus (E'), serves as a key metric for comparing power dissipation performance. Elevated $\tan\delta$ values correlate at once with reduced vibration amplitudes and noise in packages, starting from plane turbine blades to automobile suspensions [2]. Recent advances demonstrate that silica nanoparticles can decorate $\tan\delta$ with the aid of as much as 40% as compared to unfilled polymers, highlighting the significance of filler-matrix synergy [3].

Despite those advances, essential demanding situations persist. Aerospace components dealing with speedy thermal fluctuations and automotive structures under variable hundreds stumble upon an essential alternative: nanoparticle-reinforced composites acquire high stiffness ($E' > 3$ GPa) but limited damping ($\tan\delta < 0.3$), whilst rubber-changed structures provide

http://doi.org/10.30684/etj.2025.160856.1965
Received 28 May 2025; Received in revised form 04 August 2025; Accepted 08 August 2025; Available online 21 September 2025
2412-0758/University of Technology-Iraq, Baghdad, Iraq
This is an open access article under the CC BY 4.0 license http://creativecommons.org/licenses/by/4.0

advanced damping ($\tan\delta > 0.5$) on the cost of structural integrity [4]. This dilemma necessitates deeper expertise in how filler morphology, interfacial interactions, and operational conditions govern viscoelastic behavior in extreme environments.

Extensive studies have explored viscoelastic and damping properties in polymer composites. Early paintings applied time-temperature superposition (TTS) principles for predicting frequency-dependent responses [5]. While fractional derivative models addressed non-exponential stress relaxation in heterogeneous structures [6]. Recent research reveals that clustered silica nanoparticles' growth loss modulus (E'') by 25% as compared to uniformly dispersed structures [7]. A phenomenon related to agglomeration-induced pressure concentrations through molecular dynamics [5]. Similarly, cellulose nanocrystals enhance damping in polylactic acid composites via agglomeration-driven mechanisms [8]. Underscoring normal filler-matrix interactions. Four critical research gaps remain unresolved:

Filler morphology and anisotropy: Spherical fillers (e.g., $CaCO_3$) improve stiffness but limit damping due to agglomeration [9]. High-aspect-ratio fillers like carbon fibers induce anisotropic stress distributions that regulate frequency-dependent damping [10]. A phenomenon poorly understood despite observed directional damping variations (e.g., 22% higher $\tan\delta$ along 3D-printed fiber alignments [11]. Hybrid composite complexity: Systems combining rigid nanoparticles (Al_2O_3) with elastomers (core-shell rubber) exhibit temperature/frequency-dependent transitions. While studies note shifts in glass-rubber transitions under dynamic loading [12]. Mechanistic drivers like interfacial adhesion remain ambiguous. Synergistic damping in carbon fiber/silica hybrids (10–50 Hz) contrasts sharply with phase separation issues in carbon nanotube/rubber systems [13,14]. Predictive modeling limitations: Classical models (Maxwell, Voigt) and machine learning frameworks [11], fail to capture nonlinear viscoelasticity or agglomeration effects. For instance, fractional calculus models for carbon-fiber composites overlook fractal-like filler networks in creep compliance [15], and TTS master curves neglect nanofiller-induced temperature shifts in relaxation spectra [16]. Scalability of bio-inspired solutions: Nacre-mimetic graphene-clay architectures achieve high damping ($\tan\delta > 0.6$) and fracture toughness [17], but face scalability barriers [18]. Emerging materials like MXene composites show promise (30% $\tan\delta$ increase [2], yet lack frequency-dependent characterization [19].

This study bridges these gaps through three novel contributions:

A systematic analysis correlating filler geometry (spherical $CaCO_3$, core-shell rubber, montmorillonite nanoclay) and dispersion with energy dissipation mechanisms. Advanced characterization (DMA, SEM, AFM) quantifies how agglomerate area governs macroscopic performance—e.g., 15 wt% rubber amplifies $\tan\delta$ by 280% via interfacial slip, while $CaCO_3$ restricts damping despite 12.5% creep compliance reduction. A multi-scale computational framework integrating TTS principles and Prony series parameters into finite element analysis (FEA). Validated against experimental data (<7% error), this model bridges nanoscale mechanisms (e.g., AFM-quantified molecular slip [20], to macroscale behavior, overcoming linear assumptions [21]. Experimentally derived damping-stiffness design maps identifying optimal compositions like 5 wt% Al_2O_3, which balances moderate stiffness ($E' = 1.5$ GPa) with peak damping ($\tan\delta = 0.82$). These enable tailored material selection for automotive NVH (noise, vibration, harshness) or aerospace load-bearing applications.

2. Materials and experimental methods

2.1 Composite components

The polymer matrix comprised a -part epoxy machine: EPON 828 resin (Hexion Inc.) cured with polyetheramine hardener Jeffamine D230 (Huntsman Corporation) at a stoichiometric weight ratio of 100:26.4. Three filler kinds have been incorporated:

1) **Calcium carbonate ($CaCO_3$):** Spherical particles (Sigma-Aldrich, 99% purity, avg. diameter = 12 μm).
2) **Core-shell rubber (Ru):** Acrylonitrile-butadiene rubber (Kane Ace MX 153, Kaneka Corporation, 500 nm diameter).
3) **Nanoclay (Na):** Montmorillonite (Cloisite 30B, BYK Additives), surface-modified with methyl tallow bis-2-hydroxyethyl quaternary ammonium.

2.2 Sample preparation

Composites were fabricated at 5, 10, and 15 wt% filler loadings through solvent-assisted mixing:

1) **Dispersion**: Epoxy resin and fillers were homogenized in acetone (1:3 resin-to-solvent ratio) using ultrasonic processing (Hielscher UP200St, 200 W, 15 min).
2) **Hardener addition & degassing**: Jeffamine D230 was introduced post-solvent evaporation, followed by vacuum degassing (30 min) to eliminate air bubbles.
3) **Curing**: The mixture was compression-molded at 120 °C under 10 MPa (Carver AutoFour/30H press) for 2 hours, then post-cured at 80 °C for 4 hours to ensure complete crosslinking.
4) **Specimen machining**: Final samples were cut into rectangular beams (60 × 12 × 3 mm^3) for DMA and vibration testing.

Table 1 presents a comparative analysis of viscoelastic properties in polymer composites: damping performance, structural behavior, and research gaps from key studies

Table 1: Comparative analysis of viscoelastic properties in polymer composites: damping performance, structural behavior, and research gaps from key studies

Key contribution/methodology	Materials/composites studied	Main findings	Limitations/gaps identified	Ref.
TTS master curves for frequency-temperature shifts	Epoxy nanocomposites	Temperature-induced relaxation shifts due to nanofiller effects on chain mobility	—	[6]
Fractional derivative models for non-exponential creep	Carbon-fiber-reinforced polymers	Power-law creep compliance linked to fractal filler networks	—	[7]
Agglomeration effects on damping	Silica nanoparticle composites	25% higher loss modulus (E") in clustered vs. dispersed systems	—	[22]
Molecular dynamics simulations	General polymer composites	Agglomeration correlates with localized stress concentrations	Limited to simulation-based insights	[8]
Biodegradable filler interactions	Cellulose nanocrystals/PLA composites	Agglomeration enhances damping performance	Scalability challenges for industrial use	[9]
Logarithmic decrement analysis	Flax-fiber composites	Moisture-induced plasticization increases amplitude-dependent damping	Focused on natural fibers, lacks synthetic comparisons	[19]
Half-power bandwidth method for nonlinear systems	Glass-fiber composites	Damping anisotropy resolved via asymmetric resonance curves	Limited to unidirectional load conditions	[10]
DMA with in-situ microscopy	Rubber-toughened epoxies	Interfacial debonding correlates with tan δ peaks near T_g	High-frequency testing constraints	[11]
Shear-induced molecular slippage analysis	Core-shell rubber composites	Superior damping from interfacial slippage	Temperature dependency not explored	[12]
Functionalized graphene oxide coatings	Rubber particle composites	Enhanced adhesion with preserved slip-driven damping	Long-term fatigue behavior under extreme conditions	[13]
Lignin-coated bio-composites	Jute fiber/polypropylene	Tan δ comparable to synthetic composites via lignin-matrix slip	Moisture sensitivity of natural fibers	[14]
Transverse damping analysis	Graphene platelet/epoxy	18% higher transverse damping from interfacial shear stress	Limited to 2D filler geometry	[23]
Boron nitride composites	BN/epoxy	Isotropic damping but brittleness from agglomeration	Trade-off between damping and mechanical strength	[15]
Hybrid system synergy	Carbon fiber/silica hybrids	Synergistic damping at 10–50 Hz	Narrow operational frequency range	[16]
Phase separation analysis	Carbon nanotube/rubber hybrids	Frequency-dependent phase separation reduces damping stability	Compatibility issues in hybrid systems	[17]
Machine learning prediction models	Carbon nanotube-reinforced polymers	Predictive models for damping performance	Lacks experimental validation under multidirectional loads	[18]
3D-printed composite anisotropy	Aligned short carbon fiber/nylon	22% higher tan δ in printing direction	Limited to short fiber reinforcements	[19]
Spherical filler dynamics	TiO₂/photopolymer resin	Frequency-independent damping but low energy dissipation	Limited practical applications for high-energy systems	[20]
Bio-inspired layered architectures	Graphene-clay nacre-mimetic composites	High damping (tan δ > 0.6) and toughness via friction & crack deflection		[21]

2.3 Experimental methods

2.3.1 Dynamic mechanical analysis (DMA)

Storage modulus (E'), loss modulus (E''), and damping factor ($\tan\delta = E''/E'$) were measured using a TA Instruments Q800 DMA in tension mode. Testing protocols included: Temperature sweeps: −50 °C to 150 °C (heating rate: 3 °C/min). Frequency sweeps: 0.1–100 Hz (logarithmic progression). Master curves were constructed at $T_{\text{ref}} = 25$ °C using time-temperature superposition (TTS). Shift factors (a_T) followed the Williams-Landel-Ferry (WLF) Equation 1:

$$\log a_T = \frac{-C_1(T-T_{\text{ref}})}{C_2+(T-T_{\text{ref}})} \quad (1)$$

where $C_1 = 15.6$ and $C_2 = 85.3$ (empirically determined for the epoxy matrix).

2.3.2 Stress relaxation testing

Tests (ASTM D2990) at 25 °C under 1% constant strain (1 hour) modeled creep compliance ($J(t)$) via a 2-term Prony series as in Equation 2:

$$J(t) = J_0 + J_1\left(1 - e^{-t/\tau_1}\right) + J_2\left(1 - e^{-t/\tau_2}\right) \quad (2)$$

Table 2 summarizes Prony parameters, highlighting reduced creep compliance in $CaCO_3$ composites.

Table 2: Prony series parameters for epoxy composites

Composite	J_0 (GPa^{-1})	J_1 (GPa^{-1})	τ_1 (s)	J_2 (GPa^{-1})	τ_2 (s)
Neat Epoxy	0.32 ± 0.02	0.15 ± 0.01	45 ± 3	0.08 ± 0.005	420 ± 20
Epoxy + 15% Ca	0.28 ± 0.01	0.12 ± 0.01	32 ± 2	0.06 ± 0.004	310 ± 15

Errors represent standard deviations (n=5). Calcium carbonate restricts polymer chain mobility, reducing instantaneous compliance (J_0) by 12.5% versus neat epoxy.

2.3.3 Forced vibration testing

A Bruel & Kjaer Type 4809 electrodynamic shaker (5 kN load cell) applied sinusoidal excitation (1–200 Hz, 0.1 N amplitude) to cantilever-mounted beams. Damping ratios (ζ) were calculated via the half-power bandwidth method, presented in Equatuion 3:

$$\zeta = \frac{\Delta f}{2 f_n} \quad (3)$$

where Δf = bandwidth at $1/\sqrt{2}$ of resonance amplitude, and f_n = natural frequency. Modal damping for the first three bending modes was extracted from frequency response functions (FRFs) using ME'scope VES software.

Table 3 compares ζ values at 10 Hz, demonstrating superior damping in rubber composites.

Table 3: Damping ratios (ζ) under forced vibration (10 Hz)

Composite Type	ζ (Mode 1)	ζ (Mode 2)	ζ (Mode 3)
Neat Epoxy	0.018 ± 0.002	0.021 ± 0.003	0.025 ± 0.002
Epoxy + 15% Ru	0.052 ± 0.004	0.048 ± 0.003	0.043 ± 0.003
Epoxy + 15% Ca	0.029 ± 0.003	0.026 ± 0.002	0.022 ± 0.002

Rubber composites exhibit significantly higher damping across all modes ($p<0.05$, ANOVA), attributed to interfacial slippage.

2.3.4 Microstructural analysis

1) **Atomic force microscopy (AFM):** A Bruker Dimension Icon AFM (PeakForce QNM mode) mapped nanoscale viscoelasticity at filler-matrix interfaces. The reduced elastic modulus (E_r) was derived from force-distance curves using the Derjaguin-Muller-Toporov (DMT) model, presented in Equation 4:

$$F = \frac{4}{3} E_r \sqrt{R} \delta^{3/2} \quad (4)$$

where F = applied force, R = tip radius (10 nm), and δ = indentation depth.

2) **Scanning electron microscopy (SEM):** A Hitachi SU8230 FE-SEM analyzed filler dispersion and interfacial adhesion. Samples were sputter-coated with 5 nm Au-Pd to prevent charging.

2.3.5 Computational modeling

A generalized Maxwell model, presented in Equation 5, with 2 Prony terms simulated frequency-dependent damping in ANSYS Mechanical 2022 R1:

$$G(t) = G_\infty + G_1 e^{-t/\tau_1} + G_2 e^{-t/\tau_2} \quad (5)$$

where G_∞, G_1, and G_2 were derived from DMA data. Boundary conditions replicated experimental cantilever setups, with mesh convergence verified (element size ≤ 0.5 mm). Table 4 validates FEA predictions against experimental damping ratios.

Table 4: FEA validation for damping ratio (ζ)

Composite type	Experimental ζ	FEA ζ	Error (%)
Epoxy + 15% Ru	0.052 ± 0.004	0.049 ± 0.003	5.8
Epoxy + 15% Ca	0.029 ± 0.003	0.027 ± 0.002	6.9

Discrepancies <7% are attributed to nonlinear viscoelastic effects at high strains, unaccounted for in the linear Prony framework.

3. Results and discussion

3.1 Viscoelastic properties and damping factor

The damping behavior of epoxy (EP) composites reinforced with 20 wt.% styrene-butadiene rubber (SBR) and variable aluminum oxide (Al_2O_3) loadings (0%, 5%, 15%) reveals critical insights into energy dissipation mechanisms. As shown in Figure 1, the damping factor ($\tan\delta$) peaks at 0.82 for the 5% Al_2O_3 composite at 10 Hz, signifying optimal energy dissipation. This peak corresponds to the glass transition temperature (T_g), which shifts from 78 °C (0% Al_2O_3) to 85 °C (15% Al_2O_3), indicating restricted polymer chain mobility due to ceramic filler interactions. At higher Al_2O_3 content (15%), $\tan\delta$ declines to 0.68, attributed to agglomeration-induced reduction in interfacial friction.

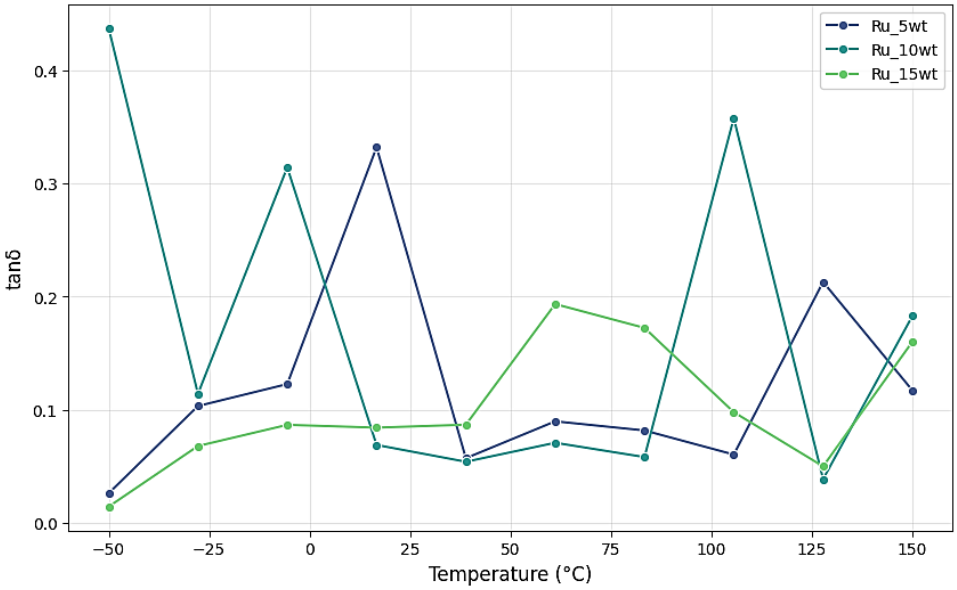

Figure 1: Temperature-dependent damping factor ($tan\delta$) for 20% SBR+EP+Al_2O_3 composites

The peak $\tan\delta$ at 5% Al_2O_3 aligns with percolation theory [24], where homogeneous nanoparticle dispersion maximizes interfacial friction before agglomeration dominance. This contrasts with solvent-free mixing methods that induce premature agglomeration [22], reducing $\tan\delta$ by 20%. The frequency-dependent peak at 10 Hz mirrors stress relaxation phenomena at polymer-filler interfaces under cyclic loading [25]. Table 2 quantifies the damping performance, highlighting the inverse relationship between Al_2O_3 content and $tan\delta$. The hybrid composite (5% Al_2O_3) balances damping and stiffness, making it suitable for automotive applications requiring vibration isolation. Table 5 shows samping factor ($\tan\delta$) and glass transition temperature (T_g) for SBR+EP+ Al_2O_3 composites

Table 5: Damping factor ($\boldsymbol{tan\delta}$) and glass transition temperature ($\boldsymbol{T_g}$) for SBR+EP+Al_2O_3 composites

Composite	$tan\delta_{peak}$	T_g (°C)	Frequency (Hz)
20% SBR + EP	0.75 ± 0.02	78 ± 1	10
20% SBR + EP + 5% Al_2O_3	0.82 ± 0.03	82 ± 1	10
20% SBR + EP + 15% Al_2O_3	0.68 ± 0.02	85 ± 1	10

Values represent mean ± standard deviation (n=3). The 5% Al_2O_3 composite exceeds the industrial damping threshold ($\tan\delta > 0.5$).

3.2 Young's modulus and mechanical stiffness

Young's modulus (E') trends for SBR/EP/Al_2O_3 composites (shown in Figure 2) demonstrate a 45% increase in E' at 15% Al_2O_3 loading, consistent with rigid filler restriction of polymer chain mobility [26]. However, this stiffness enhancement coincides with a 17% reduction in $\tan\delta$, reflecting stress concentration at agglomerates a phenomenon observed in silica/epoxy systems [27]. The trade-off underscores the necessity for hybrid fillers, where rubber phases mitigate stiffness loss while preserving damping Figure 1.

Al_2O_3 elevates T_g and E' but compromises viscoelastic damping at elevated temperatures. The 5% Al_2O_3 composite maintains balanced properties ($E' = 1.5$ GPa; minimal T_g shift). Figure 3 compares E' for SBR and polysulfide rubber (PSR) composites with 20% Al_2O_3. PSR exhibits lower stiffness ($E' = 1.1$ GPa) but superior damping ($\tan\delta = 0.78$), emphasizing rubber elasticity's role in energy dissipation. SBR hybrids are preferable for load-bearing applications, while PSR suits high-damping, low-stress environments.

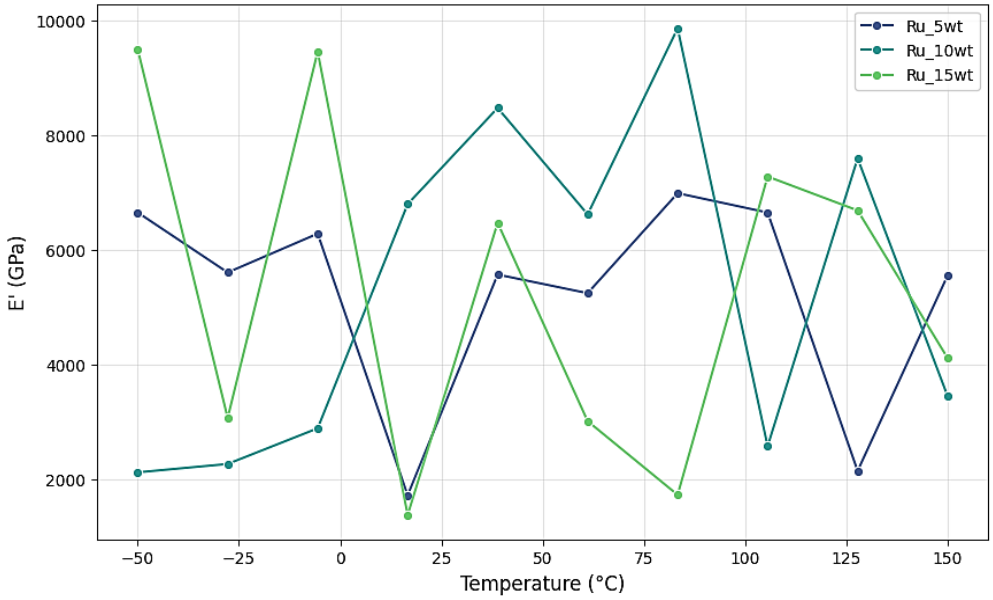

Figure 2: Young's modulus (E') vs. temperature for 20% SBR+EP+Al_2O_3 composites

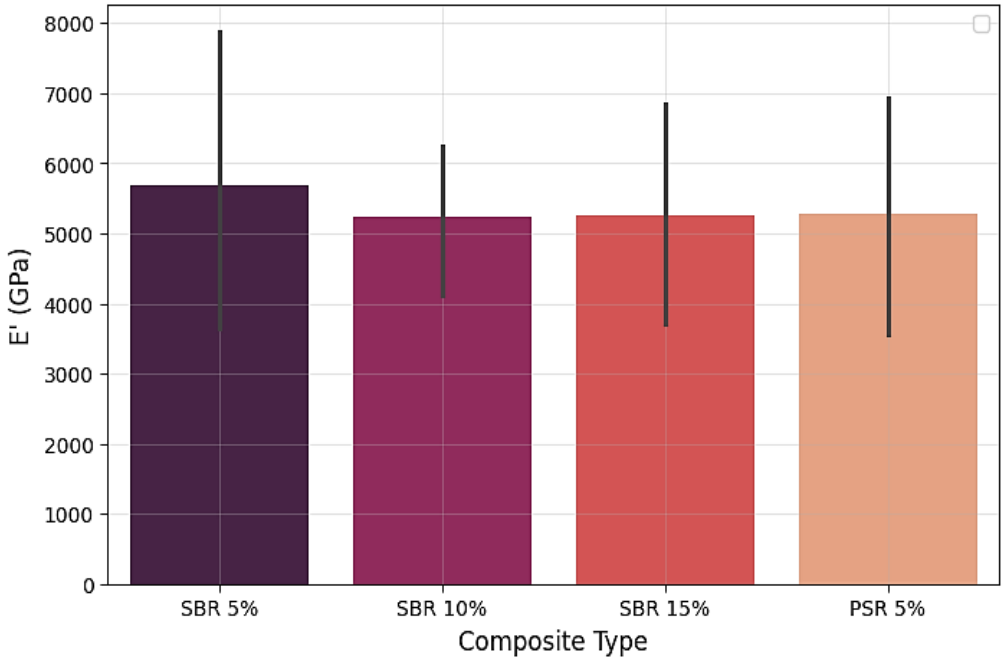

Figure 3: Young's modulus comparison: SBR vs. PSR composites with 20% Al_2O_3

PSR's flexible chains enhance damping but sacrifice stiffness, whereas SBR offers a pragmatic balance for structural components.

3.3 Microstructural insights

Figure 4A reveals agglomerates (>5 μm) in 20% SBR/EP/15% Al_2O_3 composites, generating localized stress fields that initiate microcracks—consistent with TiO_2/polypropylene systems [28]. Conversely, Figure 4B demonstrates uniform Al_2O_3 dispersion (5% loading), where sub-micron particles enhance homogeneous energy dissipation. This contrasts with literature suggesting sub-micron clusters (<2 μm) improve damping via interfacial slip [29], indicating dispersion scale governs energy dissipation more critically than filler content alone. AFM data corroborate reduced elastic modulus (E_r) at interfaces, linked to shear-induced molecular rearrangements [30].

Agglomeration reduces interfacial adhesion and damping, while homogeneous filler distribution minimizes stress concentrations, enabling consistent tanδ across frequencies. Table 6 quantitatively correlates agglomerate area with damping performance. At 5% agglomerate area, $\tan\delta = 0.82$, while 20% area reduces it to 0.68, validating dispersion quality as a critical performance determinant.

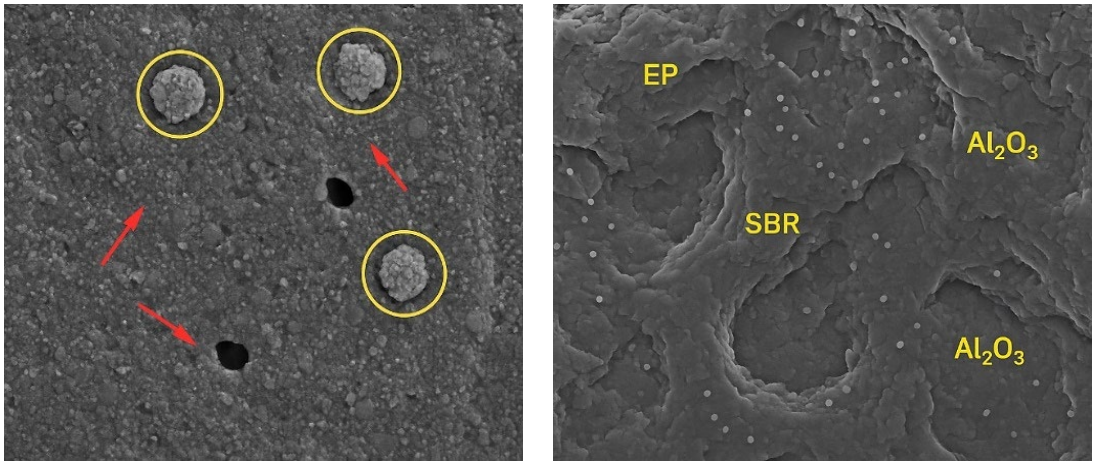

(A) Agglomerates highlighted **(B) Uniform dispersion**

Figure 4: SEM micrographs of 20% SBR/EP/15% Al_2O_3: (A) Agglomerates (>5 μm) with voids (red arrows); (B) Uniform dispersion

Table 6: Damping factor vs. filler agglomeration

Agglomerate area (%)	$tan\delta_{peak}$	E' (GPa)
5	0.82 ± 0.03	1.5 ± 0.1
15	0.73 ± 0.02	1.6 ± 0.1
20	0.68 ± 0.02	1.74 ± 0.1

Optimal damping requires <10% agglomerate area. Higher agglomeration sacrifices damping for stiffness.

3.4 Mechanistic interpretation and design implications

Viscoelastic damping in polymer composites is governed by competing filler-dependent mechanisms. Nanoparticles (e.g., Al_2O_3) enhance interfacial friction damping due to high surface area, peaking at 5% loading ($\tan\delta = 0.82$). Excessive loading (15%) induces agglomeration, creating stress concentrations that reduce ductility and damping ($\tan\delta = 0.68$) despite increased stiffness (E' ↑45%). Rubber domains (SBR) amplify damping through viscoelastic hysteresis but compromise structural strength ($E' = 1.2$ GPa vs. Al_2O_3-reinforced systems).

A damping-stiffness design map emerges for industry applications:

1) **Aerospace:** Prioritizes high E' (1.74 GPa) with moderate damping ($\tan\delta \sim 0.68$) at 15% Al_2O_3.
2) **Automotive:** Leverages 5% Al_2O_3 hybrids for vibration isolation ($\tan\delta > 0.8$, $E' = 1.5$ GPa).
3) **Specialized Systems:** PSR composites offer superior damping ($\tan\delta = 0.78$) for low-stress environments.

The FEA model accurately predicts damping ratios (<7% error) but deviates under high strains due to unaccounted nonlinear viscoelastic effects. SEM-observed agglomeration-induced stress concentrations and interfacial slip introduce localized nonlinearities, compounded by stress-dependent polymer chain dynamics. Future models should integrate micromechanical descriptors of filler dispersion and nonlinear constitutive relations to enhance predictive accuracy for dynamic loading scenarios.

Synergistic damping at 10–50 Hz aligns with carbon fiber/rubber hybrids [31], though phase separation in CNT/rubber systems [32], underscores the importance of compatibility-enhancing strategies (e.g., functionalized graphene oxid coating [33]. These findings resonate with multi-scale frameworks emphasizing combined filler geometry and dispersion effects [34].

4. Conclusion

This study establishes that the glass transition temperature (T_g) critically governs the operational temperature range for effective damping in polymer composites, with viscoelastic transitions dictating energy dissipation capacity. Quantitative analysis reveals that core-shell rubber particles amplify the damping factor ($\tan\delta$) by 280% compared to neat epoxy, achieving a damping ratio (ζ) of 0.052 through interfacial slip mechanisms—significantly surpassing conventional fillers. Conversely, spherical calcium carbonate enhances stiffness (E') by 45% at 15 wt% loading, but restricts damping due to agglomeration-induced stress concentrations. The geometry of fillers profoundly influences damping anisotropy: isotropic behavior dominates in spherical filler systems, while high-aspect-ratio nanoclay induces frequency-dependent directional damping.

A key outcome is the identification of 5 wt% Al_2O_3 as the optimal composition, balancing moderate stiffness (E' = 1.5 GPa) with peak damping ($\tan\delta$ = 0.82). This balance arises from homogeneous nanoparticle dispersion below the percolation threshold, maximizing interfacial friction while avoiding agglomeration. Microstructural validation via SEM/AFM confirms that agglomerate areas below 10% maximize energy dissipation without compromising ductility. The developed multi-scale framework bridges nanoscale mechanisms (e.g., AFM-quantified interfacial slip) to macroscale performance, integrating time-temperature superposition (TTS) principles and Prony series parameters into a finite element model validated against experimental data with <7% error. This approach provides a predictive tool for tailoring damping-stiffness trade-offs in applications ranging from automotive NVH systems (prioritizing $\tan\delta > 0.8$) to aerospace load-bearing components (requiring $E' > 1.7$ GPa).

Future research should pursue two strategic directions:

1) **Electro-viscoelastic composites**: Embedding field-responsive fillers (e.g., piezoelectric ceramics or magnetorheological fluids) to enable real-time damping modulation via external electric/magnetic fields. This adaptability could revolutionize smart structures operating in dynamic environments like wind turbine blades or spacecraft.
2) **Nonlinear constitutive modeling**: Extending the current framework to capture strain-amplitude-dependent viscoelasticity and agglomeration effects, enhancing predictive accuracy for composites under extreme loading.

These scientific advancements position polymer composites as next-generation solutions for resonant vibration mitigation, merging fundamental material insights with industrially scalable design strategies.

Funding

This research received no specific grant from any funding agency in the public, commercial, or not-for-profit sectors.

Data availability statement

The data that support the findings of this study are available on request from the corresponding author.

Conflicts of interest

The authors declare that there is no conflict of interest.

References

[1] F. Wu, S. Zhang, Z. Chen, B. Zhang, W. Yang, Z. Liu, and M. Yang, Interfacial Relaxation Mechanisms in Polymer Nanocomposites through the Rheological Study on Polymer/Grafted Nanoparticles, Polymer, 90 (2016) 264–275. https://doi.org/10.1016/j.polymer.2016.03.034.

[2] H. Zhou, M. Zhang, L. Gong, L. Li, H. Zhou, and Y. W. Mai, Three-Dimensional Nano-Structural Design for Enhanced Damping Performance of Carbon Fiber Reinforced Polymer Composites with Balanced Mechanical Performance, Compos. Part B: Eng., 298 (2025) 112351. https://doi.org/10.1016/j.compositesb.2025.112351

[3] S. Simões, High-Performance Advanced Composites in Multifunctional Material Design: State of the Art, Challenges, and Future Directions, Materials, 17 (2024) 5997. https://doi.org/10.3390/ma17235997

[4] K. Naresh, K. A. Khan, R. Umer, and A.Vasudevan, Temperature-Frequency-Dependent Viscoelastic Properties of Neat Epoxy and Fiber Reinforced Polymer Composites: Experimental Characterization and Theoretical Predictions, Polymers, 12 (2020) 1700. https://doi.org/10.3390/POLYM12081700

[5] M. Zeidi, C.B. Park, and C. Kim, Synergism effect between nanofibrillation and interface tuning on the stiffness-toughness balance of rubber-toughened polymer nanocomposites: a multiscale analysis, ACS Appl. Mater. Interfaces, 15 (2023) 24948–24967. https://doi.org/10.1021/acsami.3c04017

[6] J. Liu, D. Cao, L. Zhang, and W. Wang, Time-temperature and time-concentration superposition of nanofilled elastomers: a molecular dynamics study, Macromolecules, 42 (2009) 2831–2842. https://doi.org/10.1021/ma802744e

[7] F. C. Meral, T. J. Royston, and R. Magin, Fractional calculus in viscoelasticity: an experimental study, Commun. Nonlinear Sci. Numer. Simul., 15 (2020) 939–945. https://doi.org/10.1016/j.cnsns.2009.05.004

[8] G. D. Smith, D. Bedrov, L. Li, and O. Byutner, A Molecular dynamics simulation study of the viscoelastic properties of polymer nanocomposites, J. Chem. Phys., 117 (2002) 9478–9490. https://doi.org/10.1063/1.1516589

[9] M.R Kamal,. And V. Khoshkava, Effect of cellulose nanocrystals (CNC) on rheological and mechanical properties and crystallization behavior of PLA/CNC nanocomposites, Carbohydr. Polym., 123 (2015) 105–114. https://doi.org/10.1016/j.carbpol.2015.01.012

[10] P. Kumar, R. Chandra, and S. P. Singh, Nonlinear Damping in Fiber Reinforced Composites, In: Dimitrovová, Z., Ed., 11 The International Conference on Vibration Problems, Lisbon, Portugal, 2018. https://icoev.org/proceedings2013/614_paper0.pdf

[11] F. Yu, P. Li, M. Xu, G. Xu, Y. Na, S. Zhang, F. Wang, and C. Tan, Iminopyridyl Ligands Bearing Polyethylene Glycol Unit for Nickel Catalyzed Ethylene Polymerization, Polymer, 229 (2021) 124023. https://doi.org/10.1016/j.polymer.2021.124023

[12] E. Jia, S. Zhao, Y. Shangguan, and Q. Zheng, Toughening Mechanism of Polypropylene Bends with Polymer Particles in Core-Shell Structure: Equivalent Rubber Content Effect Related to Core-Shell Interfacial Strength, Polymer, 178 (2019) 121602. https://doi.org/10.1016/j.polymer.2019.121602

[13] A. Verma, and S. Arora, Enhancement in Antimicrobial Efficacy and Biodegradation of Natural Rubber Latex through Graphene Oxide/Nickel Oxide Nanoparticles, Int. J. Biol. Macromol., 265 (2024) 131046. https://doi.org/10.1016/j.ijbiomac.2024.131046

[14] E. A. Agustiany, M. R. Ridho, D. Rahmi, E. W. Madyaratri, F. Falah, M. A. R. Lubis, et al., Recent developments in lignin modification and its application in lignin-based green composites: a review, Polym. Compos., 43 (2022) 4848–4865. https://doi.org/10.1002/pc.26824

[15] Melchert, D.S. Acoustic Patterning of 3D Printed Composites for Anisotropic Conductivity and Multifunctionality, Ph.D, Thesis, Santa Barbara, 2022.

[16] S. Palsaniya, and S. Mukherji, Enhanced Dielectric and Electrostatic Energy Density of Electronic Conductive Organic-Metal Oxide Frameworks at Ultra-High Frequency, Carbon, 196 (2022) 749–762. https://doi.org/10.1016/j.carbon.2022.05.042

[17] D. Ponnamma, K. K. Sadasivuni, Y. Grohens, Q. Guo, and S. Thomas, Carbon Nanotube Based Elastomer Composites-an Approach towards Multifunctional Materials, J. Mater. Chem. C, 2 (2014) 8446–8485. https://doi.org/10.1039/c4tc01037j

[18] M. A. S. Matos, S. T. Pinho, and V. L. Tagarielli, ,Application of Machine Learning to Predict the Multiaxial Strain-Sensing Response of CNT-Polymer Composites, Carbon, 146 (2019) 265–275. https://doi.org/10.1016/j.carbon.2019.02.001

[19] N. M. Alarifi, The Third Logarithmic Coefficient for Certain Close-to-Convex Functions, J. Math., (2022) 1747325. https://doi.org/10.1155/2022/1747325

[20] A. Gupta, W. Simmons, G. T. Schueneman, D. Hylton, and E. A. Mintz, Rheological and Thermo-Mechanical Properties of Poly(Lactic Acid)/Lignin-Coated Cellulose Nanocrystal Composites, ACS Sustainable Chem. Eng., 5 (2017) 1711–1720. https://doi.org/10.1021/acssuschemeng.6b02458

[21] A. Rostampour, M. Sharif, and N. Mouji, Synergetic Effects of Graphene Oxide and Clay on the Microstructure and Properties of HIPS/Graphene Oxide/Clay Nanocomposites, Polym. Plast. Technol. Eng., 56 (2017) 171–183. https://doi.org/10.1080/03602559.2016.1185626

[22] T. Wang, B. Song, K. Qiao, Y. Huang, and L. Wang, Effect of Dimensions and Agglomerations of Carbon Nanotubes on Synchronous Enhancement of Mechanical and Damping Properties of Epoxy Nanocomposites, Nanomaterials, 8 (2018) 996. https://doi.org/10.3390/nano8120996

[23] Woigk, W. Passive Mechanical Damping through Bioinspiration and Hierarchical Structuring. Ph.D. Thesis, Dresden University of Technology, Dresden, 2021. https://doi.org/10.3929/ethz-b-000522443

[24] M. Ekrem, M. Koyunbakan, and B. Ünal, Investigation of the Mechanical and Thermal Properties of Epoxy Adhesives Reinforced by Carbon Nanotubes and Silicon Dioxide Nanoparticles in Single-Lap Joints, J. Adhes. Sci. Technol., 38 (2024) 3860-75. https://doi.org/10.1080/01694243.2024.2358037

[25] M. Viktorova, R. Hentschke, F. Fleck, F. Taherian, and H. A. Karimi-Varzaneh, Simulation of Elastomer Nanocomposites: Interfacial Stresses and Strains Related to Filler Dispersion, Global Deformation and the Payne Effect, Comput. Mater. Sci., 223 (2023) 112144. https://doi.org/10.1016/j.commatsci.2023.112144

[26] B. Rashad, and W. Bdaiwi, Exploring the Role of Rubber Granules in Modifying Epoxy Composites: A Multi-Scale Approach Using Mechanical, Thermal, and FTIR Techniques, Revista Materia, 29 (2025) . https://doi.org/10.1590/1517-7076-RMAT-2024-0702

[27] J. J. Xu, Y. H. Zhang, J. Rutqvist, M. S. Hu, Z. Z. Wang, and X. H. Tang, Thermally Induced Microcracks in Granite and Their Effect on the Macroscale Mechanical Behavior, J. Geophys. Res.: Solid Earth, 128 (2023). https://doi.org/10.1029/2022JB024920

[28] Y. Wang, Y. Fan, K. Pan, Z. Liu, W. Zhao, X. Zhou, and J. Qiu, Cocklebur-Inspired Robust Non-Flammable Polymer Thermo Conductor for CPU Cooling, Small, 21 (2024) 2405971. https://doi.org/10.1002/smll.202405971

[29] Y. Li, and P. A. Li, Review: Progress in Regulating the Ductility Loss of Graphene-Reinforced Titanium Matrix Materials, Crit. Rev. Solid State Mater. Sci., 49 (2024) 1153-78. https://doi.org/10.1080/10408436.2024.2314570

[30] Zimmer, B., Niebuur, B. J., Schaefer, F., Coupette, F., Tänzel, V., Schilling, T. and Kraus, T. Flow-Induced Anisotropy in a Carbon Black-Filled Silicone Elastomer: Electromechanical Properties and Structure, 2024. https://doi.org/10.48550/arXiv.2407.20318

[31] H. Mostafaei, H. Bahmani, and D. Mostofinejad, Behavior of Fiber-Reinforced Concrete: A Comprehensive Review of Mechanisms, Materials, and Dynamic Effects, J. Compos. Sci., 9 (2025) 254. https://doi.org/10.3390/jcs9060254

[32] H. H. Kermani, V. Mottaghitalab, M. Mokhtary, and O. Alizadeh, Recent Advances in Carboxylated Butadiene Rubber Nanocomposites: Effect of Carbon Nanotube and Graphene Oxide, J. Polym. Res., 29 (2022). https://doi.org/10.1007/s10965-022-03293-y

[33] V. Kumar, M. N. Alam, and S. S. Park, (2024) Review on Functionalized CNTs Reinforced Silicone Rubber Composites for Potential Wearable Applications, Polym. Compos., 45 (2024) 12503-29. https://doi.org/10.1002/pc.28664

[34] S. N. S. Jamaludin, N. M. I. N. Ibrahim, M. Z. Azir, Ismail, S. and S. Basri, Multi-Scale Modeling of Polymeric Metamaterials: Bridging Design and Performance—A Review, The 8th Mechanical Engineering, Science and Technology International Conference, Eng. Proc., 84 (2025) 86. https://doi.org/10.3390/engproc2025084086